HHS Public Access

Author manuscript

Int J Radiat Oncol Biol Phys. Author manuscript; available in PMC 2017 April 05.

Published in final edited form as:

Int J Radiat Oncol Biol Phys. 2016 November 01; 96(3): 529–537. doi:10.1016/j.ijrobp.2016.07.008.

Stereotactic Body Radiation Therapy Delivery in a Genetically Engineered Mouse Model of Lung Cancer

Shisuo Du, MD, PhD[*], **Virginia Lockamy, PhD**[*], **Lin Zhou, MD, PhD**[†], **Christine Xue, BS**[*], **Justin LeBlanc, BS, BA**[*], **Shonna Glenn, BS**[‡], **Gaurav Shukla, MS, BA**[*], **Yan Yu, PhD**[*], **Adam P. Dicker, MD, PhD**[*], **Dennis B. Leeper, PhD**[*], **You Lu, MD, PhD**[†], and **Bo Lu, MD, PhD**[*]

[*]Department of Radiation Oncology, Thomas Jefferson University, Philadelphia, Pennsylvania

[†]Department of Thoracic Oncology, Cancer Center and State Key Laboratory of Biotherapy, West China Hospital, Sichuan University, Chengdu, Sichuan, China

[‡]Xstrahl, Inc, Suwanee, Georgia

Abstract

Purpose—To implement clinical stereotactic body radiation therapy (SBRT) using a small animal radiation research platform (SARRP) in a genetically engineered mouse model of lung cancer.

Methods and Materials—A murine model of multinodular *Kras*-driven spontaneous lung tumors was used for this study. High-resolution cone beam computed tomography (CBCT) imaging was used to identify and target peripheral tumor nodules, whereas off-target lung nodules in the contralateral lung were used as a nonirradiated control. CBCT imaging helps localize tumors, facilitate high-precision irradiation, and monitor tumor growth. SBRT planning, prescription dose, and dose limits to normal tissue followed the guidelines set by RTOG protocols. Pathologic changes in the irradiated tumors were investigated using immunohistochemistry.

Results—The image guided radiation delivery using the SARRP system effectively localized and treated lung cancer with precision in a genetically engineered mouse model of lung cancer. Immunohistochemical data confirmed the precise delivery of SBRT to the targeted lung nodules. The 60 Gy delivered in 3 weekly fractions markedly reduced the proliferation index, Ki-67, and increased apoptosis per staining for cleaved caspase-3 in irradiated lung nodules.

Conclusions—It is feasible to use the SARRP platform to perform dosimetric planning and delivery of SBRT in mice with lung cancer. This allows for preclinical studies that provide a rationale for clinical trials involving SBRT, especially when combined with immunotherapeutics.

Reprint requests to: Bo Lu, MD, PhD, Department of Radiation Oncology, Thomas Jefferson University and Hospitals, 111 South 11th St, Philadelphia, PA 19107. Tel: (215) 955-6705; bo.lu@jefferson.edu.

S. Du, V. Lockamy, and L. Zhou contributed equally to this study.

Conflict of interest: none.

Introduction

Radiation therapy is part of the treatment regimen for the majority of cancer patients worldwide (1). Stereotactic body radiation therapy (SBRT), which delivers a large fractionated dose with high conformality to the targeted tumor, has emerged as a promising surrogate to conventional fractionated radiation therapy for patients with medically inoperable cancers. For instance, SBRT achieves 3-year local control rates of around 90% in stage I non-small cell lung cancer (NSCLC) (2). Prospective data suggest that its use results in survival rates comparable to those of surgery (3) and provides more than double the rate of primary tumor control compared with conventional radiation therapy.

Until recently, modern radiation therapy could not be mimicked in the preclinical setting because of the lack of sophisticated small animal irradiators. As a result, critical biological research regarding SBRT has been delayed. In particular, it has been unclear whether classic radiobiological modeling is appropriate for the large doses per fraction that SBRT delivers (4) because previous studies of small animal irradiation have used simplified treatment plans in preclinical models (5). Therefore, there is an urgent need for reliable preclinical models for SBRT that closely mirror the clinical usage of SBRT to enable an understanding of its underlying mechanisms for efficacy and its toxicities. Recently, several image guided irradiator systems have been developed to precisely irradiate small tumors in mice. These include commercial linear accelerators (6, 7), an ^{192}Ir-based small animal irradiator with an integrated micro–computed tomography scanner, a collimation system for targeted irradiation (8), and a system that uses a 225-kV gantry-mounted x-ray source (9, 10). One such system using onboard image guidance was recently used to deliver whole brain irradiation with hippocampal avoidance in a rodent model (11).

The recent development and commercialization of small animal image guided radiation therapy devices have empowered researchers to conduct preclinical investigations in a manner that more accurately reflects the clinical scenario using millimeter-sized beams. However, each of these techniques has strengths and weaknesses for simulating SBRT in humans (eg, very high dose to the focal area using precise targeting). There are still insufficient preclinical data from treating mouse lung cancer with SBRT because small target volumes are technically challenging for SBRT delivery.

Our aim in this study was to test the feasibility of applying clinical treatment planning parameters in SBRT planning and delivery to a mouse model of lung cancer. We wanted to learn the feasibility of using a small animal radiation research platform (SARRP) for SBRT planning, delivery, and response evaluation in a preclinical mouse model of spontaneous lung tumors. SARRP enabled the preclinical SBRT research because of its capability for high-resolution imaging and its accurate conformal radiation beam delivery system, which can mimic the clinical treatment machines used for SBRT delivery. Furthermore, using SARRP-enabled SBRT, we tested whether an animal model that simulates clinical tumor response in patients would generate the necessary preclinical data to guide future clinical trials of SBRT, for example, when it is combined with immunotherapy.

Methods and Materials

Spontaneous mouse lung cancer model

All studies involving mice were approved by the Thomas Jefferson University Animal Care and Use Committee. The mouse strain harboring a conditional activating mutation (G12D) at the endogenous *Kras* locus has been described previously (12). It carries a targeted latent "hit-and-run" *Kras* allele that is activated by an in vivo spontaneous recombination event, resulting in an activated allele (K-ras G12D). Mice carrying this mutation have a mean survival time of 200 days, with the lifespan limited by extensive tumor burden. Tumors are most frequently located in the lung.

Small animal radiation research platform

The SARRP is developed to perform high-resolution imaging and accurate conformal radiation therapy to target tumors in small animals. The system uses a dual-focus, 0.15-mm Cu filtration, constant voltage x-ray source operating up to 225 kVp, which is mounted on a rotating gantry with a nominal source-to-isocenter distance of 35 cm. Gantry rotation is limited to 120° from vertical at fixed 15° increments. Computer-controlled robotic translation and rotation stages are used to position the animal.

We anesthetized 3 mice with *Kras*-driven spontaneous lung tumors with ketamine (100 mg/kg) and acepromazine (2.5 mg/kg) and immobilized them on a treatment bed before radiation therapy or cone beam computed tomography (CBCT). They were individually placed on a plastic holder secured onto the 4-axis robotic positioner of the SARRP (Xstrahl, Surrey, UK) that provides both rotary motion for CBCT and translation and rotation for radiation therapy delivery. A laser alignment system was used to facilitate an accurate, reproducible setup of the subjects. All murine lung cancers were treated by use of a 5-mm collimator using 220-kVp and 13-mA photons. A weekly dose of 20 Gy was delivered continuously for 3 weeks, delivering a total dose of 60 Gy in 3 fractions.

The SARRP uses a radiation therapy planning (13), verification (14) and delivery system called MuriPlan that allows for both planning and delivering radiation therapy. The MuriPlan planningmodule enables single or multiple beams to be targeted to the isocenter and can create contours of tumors and of organs at risk to reduce dose to normal tissues.

Using the treatment planning system, we imaged and treated tumors with specific beam arrangements, similar to those used clinically. The MuriPlan dose algorithm uses a superposition-convolution algorithm that is similar to the Pinnacle3 treatment planning systems (Philips, Koninklijke Philips, Naamloze Vennootschap (N.V.)). However, whereas Pinnacle3 uses approximately 4 to 6 energy bins to capture the MV spectrum, the small animal superposition-convolution algorithm uses 25 Kernels at 10-keV bins. The small animal algorithm used a larger number of kernels so that the calculations better modeled the beam spectrum (kV energy) and presence of different filters. All of the kernels were generated using Monte Carlo simulations. The model also accommodated beam modifiers, such as independent jaws.

CBCT acquisition using the SARRP imaging subsystem

The onboard CBCT scanner was used to obtain high-resolution CT scans to image and monitor lung tumor volume before and after radiation therapy. As described (14), each mouse was rotated between the stationary x-ray source and a 2-dimensional digital flat-panel detector in a horizontal setup. The images were obtained at 60 kVp and 0.5 mA with an uncollimated primary beam, 20 cm × 20 cm at the isocenter, with a continuous beam-on and continuous stage rotation mode. A total of 360 projections were acquired at approximately 1° angular increments. To facilitate treatment planning, the CBCT slices were then rendered into a 3-dimensional (3D) reconstruction of the mouse, allowing spatial organization and localization of the tumor mass. Before each treatment, CBCT was performed to visualize the target tumor and confirm the target position.

Radiographic assessment for treatment response after SBRT

Follow-up CBCT scans were performed 4, 5, 6, 7, and 8 weeks after the first day of radiation treatment. The tumor volume was determined by contouring the tumor on the CBCT images.

Histopathology and immunochemistry

To visualize histopathologic changes in the target tumors, hematoxylin and eosin and staining for Ki-67 and cleaved caspase-3 were performed. Mouse lungs were perfused with 10% formalin, stored in fixative overnight, embedded in paraffin, and cut into 6-μm sections. Briefly, after trypsinization and incubation in formamide in trisodium citrate at 70°C for 45 min, the sections were incubated with (*1*) anti-Ki-67 (Santa Cruz Biotech, Santa Cruz, CA); (*2*) biotinylated antimouse antiplasma (Vector, Burlingame, CA); and (*3*) avidin dehydrogenase–biotinylated HRP complex (Vecstastain ABC kit, Vector) according to the instructions from the supplier. Additionally, the duplicate sections were incubated with cleaved caspase-3 antibody (Cell Signaling, Boston, MA). Nuclear reactivity was taken into account for Ki-67 staining, which was recorded as continuous variables, based on the proportion of positive tumor cells regardless of staining intensity. The Ki-67 and cleaved caspase-3 labeling index were defined as the percentage of labeled cells per high power field (HPF). For analysis of the proliferation index, 5 consecutive HPFs (×40 magnification) were examined in each of the specimens under a light microscope (Zeiss, Jena, Germany) in a blinded fashion.

Statistical analysis

Statistical analysis was performed by 2 blinded researchers. Differences between the irradiated target tumor group and the control group were evaluated using the Student *t* test where appropriate. The values are expressed as the mean ± standard deviation. A probability value of $P<.05$ is considered statistically significant.

Results

SBRT delivery through SARRP

Our goal was to use the SARRP to perform high-resolution imaging and accurate conformal beam therapy in a preclinical murine model of spontaneous lung tumors. Figure 1

recapitulates the establishment of an SBRT technique in a transgenic lung cancer model on the SARRP Xstrahl research platform. The SARRP consists of a kilovoltage xray tube producing energy beams up to 225 kVp mounted on a rotating gantry. Fluoroscopic imaging with the electronic portal imaging device can be used during irradiation for treatment localization and verification. Pretreatment onboard CBCT images were obtained (Fig. 2A) to demonstrate that the resolution was high enough to visualize the tumors for contouring, and the CBCT slices were rendered into a 3D reconstruction of the mouse (Fig. 2B) to facilitate treatment planning.

Dosimetric planning and image guided delivery of SBRT per clinical guidelines

MuriPlan, an image guided small animal dose planning system built on the same platform as the existing SARRP treatment/dose planning system, was used to develop an SBRT treatment plan similar to that for humans. The contouring package in MuriPlan specified the following organs at risk (OARs) as specified by RTOG 0813: spinal cord, esophagus, heart, trachea, lungs, skin, and great vessels. Tumor location is a crucial factor for SBRT in lung cancer. In the initial phase 1 lung SBRT study, the treatment of tumors near the proximal bronchial structures produced an 11-fold increase in toxicity relative to tumors located more peripherally (15). This was largely caused by atelectasis occurring downstream from irradiated primary bronchi and bronchioles. For this reason, central tumors were specifically excluded from RTOG 0236 (16), and the dose was reduced significantly in RTOG 0618. In our model, we sought to target a single tumor within the middle or the lower lobe of peripheral lung. A single peripheral tumor 2 to 3 mm in diameter was selected to delineate the gross tumor volume (GTV) in each mouse. To account for breathing and the geometric uncertainty, a 5 × 5 mm collimator was selected to encompass the tumor volume. A 1-mm to 2-mm expansion was added to the GTV to form the planning target volume (PTV). The prescribed dose of 60 Gy, chosen on the basis of clinical trials for humans, was delivered in 3 fractions of 20 Gy each to the mouse lung tumor (17).

Close resemblance to radiation therapy delivery in humans was achieved using 7 to 10 nonoverlapping, nonopposing beams chosen with at least 3 noncoplanar beams to enhance conformity of dose spillage (Fig. 3A). The beam arrangement consisted of 5 × 5–mm diameter noncoplanar x-ray beams chosen to avoid direct irradiation of the spinal cord and to spare the other OARS as much as possible. The isocenter was placed in themiddle of the tumor, and a 5 × 5–mm collimator was used to encompass the tumor volume. In the first group of 3D plans, a single isocenter was placed centrally within the tumor volume. The second group of 3D plans consisted of multiple isocenters placed within the tumor using 5 × 5–mm diameter noncoplanar x-ray beams. This group of plans used the same gantry angles as the initial group except that these plans had multiple isocenters. The reason for the multiple isocenters is best described by Matinfar et al (18), who stated that there is no true single isocenter for the SARRP based on the 2 axes of rotation and physical factors affecting the x-ray device. They proposed either using a “best-fit” isocenter (not as accurate for the SARRP) or defining different isocenters for each gantry angle. When using multiple isocenters, the doses for the plans were prescribed to each isocenter that was used.

Multiple plans were developed and evaluated before treatment selection. The treatment plan with best dosimetry parameters listed in Figure 3 was used to treat the mice. The plans were chosen based on the similarity with current clinical practice and the ability to ensure PTV dose conformity and OAR sparing. To assess the quality of a plan, the dose-volume histogram (DVH) (Fig. 3B) and the SBRT parameters, such as ratio of prescription isodose volume to PTV(R100%), ratio of 50% prescription isodose volume to PTV(R50%), maximal dose 2 mm from the PTV in any direction as a percentage of prescription dose (D_{2mm}) and percentage of ipsilateral lung receiving dose equal to or larger than 20 Gy (V20) (Fig. 3C), were compared with the RTOG 0813 planning guidelines. In the 3 animal models used, $R_{100\%}$ ranged from 0.99 to 1.95, $R_{50\%}$ ranged from 3.96 to 5.15, D_{2mm} ranged from 31.67 to 55.9Gy, and V_{20} ranged from 3.7%to 18.5%. In addition, V_{20} values for the OARs were evaluated to minimize exposure to normal tissue.

Radiographic response to SBRT in mice

To assess the therapeutic efficacy of the SBRT plan and to determine whether the effect of SBRT on tumor volumes in mice was similar to the effect on humans, weekly CBCTs were obtained to monitor the volumes of target-irradiated tumors and control tumors in the contralateral lung. Figure 4A displays the pretreatment CBCTs and CBCTs taken 4, 5, 6, 7, and 8 weeks after the initiation of radiation therapy of a single mouse. On the CBCT images, the target tumor volume on week 6 was visibly smaller than on week 5.

Direct comparison of target and control tumor volumes during and after SBRT (Figs. 4B and 4C) was performed to assess the therapeutic efficacy of RT. Figure 4B delineates the evolution of tumor volumes during radiation therapy and the follow-up period. In all 3 models, an increase in target tumor volume was observed in weeks 1 to 3, during the course of SBRT; however, during weeks 4 to 8, the target tumor volumes decreased. By week 8, the targeted tumors decreased significantly compared with pretreatment volumes (Fig. 4C). This is in contrast to control tumors, which received minimal radiation and increased significantly in size during the 8 weeks (P=.0089). The decrease in target tumor volume in all 3 mouse models confirms that the SBRT treatment plan effectively targeted the lesions of interest.

Pathologic response to SBRT in mice

To visualize the tumors targeted by SBRT, the mice were killed 8 weeks after the initiation of radiation therapy, and the gross morphology of the target tumors after receiving doses of 60 Gy was observed. A targeted tumor in the peripheral right posterior lung is shown in Figure 5A. Gross inspection revealed a well-demarcated circular area representing the tumor, which is surrounded by lung parenchyma.

To determine whether the proliferation rate was affected upon SBRT, the target tumors were analyzed 8weeks after the initiation of radiation therapy (Fig. 5B). Using Ki-67 staining as a surrogate for the proliferation rate, we observed considerable differences in the basal proliferation between the target and control tumors. The proliferation index was defined as the percentage of Ki-67–positive cells per HPF. The proliferation index was significantly lower in target-irradiated tumors than in control tumors receiving minimal radiation (P= .039), indicating that SBRT decreased cell proliferation significantly in this model (Fig. 5D).

Cleaved caspase-3 staining was also performed as a marker for apoptotic cell death (Fig. 5C). The apoptotic index was defined as the percentage of cleaved caspase-3 positive cells per HPF. The apoptotic index was significantly higher in targeted tumors than in control tumors (P=.036), indicating that SBRT leads to apoptosis as a mechanism of cell death in this model (Fig. 5E).

Discussion

We have demonstrated that SBRT can be delivered precisely to murine peripheral lung tumors with limited exposure to adjacent tissues and OARs. Furthermore, we demonstrated that SARRP-enabled SBRT allows more relevant preclinical studies to guide future clinical trials of SBRT. Our study is unique from others using small animal irradiation systems in that it satisfies all of the following requirements: we used clinical dosimetric planning and guidelines and image guidance for precise delivery, we developed an SBRT technique that allows for treating a small mouse lung nodule using RTOG guidelines for SBRT planning, the DVH was evaluated for plan optimization based on conformality index as described in the RTOG 0813 protocol, and the small animal SBRT technique was developed on an X-RAD 320 equipped with a collimator system composed of 5-cm-thick copper to produce focal radiation beams that simulate clinical SBRT (19). As described in the RTOG 0236 clinical trial (20), 60 Gy in 3 fractions was prescribed to PTV. Cone beam CT was used for image guided radiation delivery (21). A CT scan of the entire mouse on the treatment couch was acquired immediately before each radiation delivery, which was completed and reconstructed in less than 5 minutes. The CBCT scan was then automatically registered to the treatment planning CT scan to facilitate precise repositioning of the mouse to the treatment isocenter. This allows precise delivery of SBRT.

It has been reported that in mice, large lung tumors move less than small tumors in mice during respiration, but the motion rarely exceeds 0.5 mm (20). The PTV is a geometric margin designed to account for daily setup error and target motion. Physically, a 0.45-mm penumbra was observed when using the 0.5-cm focal spot of the x-ray tube (22). To account for these uncertainties, we used a 5 × 5–mm collimator providing 1- to 2-mm margins between GTV and PTV to ensure that the prescription dose was actually delivered to the GTV. Despite delivering a higher biological dose of 20 Gy in 3 fractions without breathing control, we did not observe histologic signs of radiation acute pneumonitis, anorexia, or pleural effusions in this model, noting that an observation period of 8 weeks may not be sufficient for the development of these side effects.

Our immunocompetent mice, in which multiple tumors spontaneously develop in lung, offer various advantages, including a tumor microenvironment that better represents that of human lung cancer in the presence of intact host-immune system, which is suitable for studying the combination of SBRT and immunotherapy. Of note, the tumors in our model closely resemble the genetic and histopathologic features of human disease (23). The murine model of multinodular *Kras*-driven spontaneous lung cancer not only allows autochthonous tumor formation surrounded by a normal tissue microenvironment in an immunocompetent animal, but also offers the possibility to model any gene mutation that is relevant in human lung cancer (24). NSCLC often harbors *Kras* gene mutations, which are associated with smoking,

and it has an unfavorable prognosis (25–27). Research is lacking, however, on the radiation responsiveness and clinical outcomes after radiation therapy for the *Kras* mutation subgroups of NSCLC. Further studies of these mechanisms in this model may provide additional insights into the detrimental treatment response in this population of patients.

The dose of 20 Gy in 3 fractions produces clinical control that exceeds 90% in lung cancer patients (2), although pathologic response is unknown. In this study, we found viable cancer cells 8 weeks after the same SBRT regimen. It remains to be determined whether this is unique to this mouse model of lung cancer and whether dose escalation and use of radiosensitizers or immunotherapeutics will lead to eradication of the residual cancer cells. One particular area of research that this model may inform is the abscopal effect, in which irradiation of a target leads to a clinical response in the targeted lesion and in other lesions outside the irradiated field. This effect is thought to be mediated through the initiation of an immune response to dead cancer cells after ablative radiation doses (28). The consequences of this immune response can be beneficial (29). The precise mechanistic explanations of this effect are as yet unclear. Unfortunately, in our model, an abscopal effect after SBRT alone was not detected.

In summary, this work introduces a novel platform that can potentially bridge bench research with clinical management of lung cancer. Looking forward, we believe that combining radiation therapy with immunotherapy will break immune tolerance by the activation of antigen-presenting cells and T cells that may lead to abscopal effects. In preclinical models, promising results have been reported in the combination of radiation therapy with immune checkpoint inhibitors. With the irradiated tumor functioning as an in situ vaccine, the combination of radiation therapy and anti-CTLA-4 resulted in successful T-cell–mediated antitumor responses, whereas anti-CTLA-4 treatment by itself was ineffective (30). However, most of the data were generated from subcutaneously syngeneic tumor models, partially because the conventional irradiator does not allow precision radiation therapy for treating small internal targets. To take advantage of the established SBRT technique and NSCLC-specific genetically engineered mouse models, we plan to further investigate appropriate regimens of SBRT in terms of dose/fractionation when that regimen is combined and optimally sequenced with immunotherapeutics.

Acknowledgments

Supported in part by NIH Shared Instrumentation Grant (S10).

References

1. Schaue D, McBride WH. Opportunities and challenges of radiotherapy for treating cancer. Nat Rev Clin Oncol. 2015; 12:527–540. [PubMed: 26122185]
2. Timmerman R, McGarry R, Yiannoutsos C, et al. Excessive toxicity when treating central tumors in a phase II study of stereotactic body radiation therapy for medically inoperable early-stage lung cancer. J Clin Oncol. 2006; 24:4833–4839. [PubMed: 17050868]
3. Chang JY, Senan S, Paul MA, et al. Stereotactic ablative radiotherapy versus lobectomy for operable stage I non-small-cell lung cancer: A pooled analysis of two randomised trials. Lancet Oncol. 2015; 16:630–637. [PubMed: 25981812]

4. Brown JM, Carlson DJ, Brenner DJ. The tumor radiobiology of SRS and SBRT: Are more than the 5 Rs involved? Int J Radiat Oncol Biol Phys. 2014; 88:254–262. [PubMed: 24411596]
5. Motomura AR, Bazalova M, Zhou H, et al. Investigation of the effects of treatment planning variables in small animal radiotherapy dose distributions. Med Phys. 2010; 37:590–599. [PubMed: 20229867]
6. De Salles AA, Melega WP, Laćcan G, et al. Radiosurgery performed with the aid of a 3-mm collimator in the subthalamic nucleus and substantia nigra of the vervet monkey. J Neurosurg. 2001; 95:990–997. [PubMed: 11765845]
7. DesRosiers C, Mendonca MS, Tyree C, et al. Use of the Leksell Gamma Knife for localized small field lens irradiation in rodents. Technol Cancer Res Treat. 2003; 2:449–454. [PubMed: 14529310]
8. Graves EE, Zhou H, Chatterjee R, et al. Design and evaluation of a variable aperture collimator for conformal radiotherapy of small animals using a microCT scanner. Med Phys. 2007; 34:4359–4367. [PubMed: 18072501]
9. Wong J, Armour E, Kazanzides P, et al. High-resolution, small animal radiation research platform with x-ray tomographic guidance capabilities. Int J Radiat Oncol Biol Phys. 2008; 71:1591–1599. [PubMed: 18640502]
10. Herter-Sprie GS, Korideck H, Christensen CL, et al. Image-guided radiotherapy platform using single nodule conditional lung cancer mouse models. Nat Commun. 2014; 5:5870. [PubMed: 25519892]
11. Cramer CK, Yoon SW, Reinsvold M, et al. Treatment planning and delivery of whole brain irradiation with hippocampal avoidance in rats. PLoS One. 2015; 10:e0143208. [PubMed: 26636762]
12. Ji H, Ramsey MR, Hayes DN, et al. LKB1 modulates lung cancer differentiation and metastasis. Nature. 2007; 448:807–810. [PubMed: 17676035]
13. Brodin NP, Guha C, Tome WA. Proposal for a simple and efficient monthly quality management program assessing the consistency of robotic image-guided small animal radiation systems. Health Phys. 2015; 109:323. [PubMed: 26313591]
14. Cho NB, Kazanzides P. A treatment planning system for the small animal radiation research platform (SARRP) based on 3D Slicer. MIDAS J 2012. Available at: http://www.midasjournal.org/browse/publication/86.
15. Timmerman RD, Park C, Kavanagh BD. The North American experience with stereotactic body radiation therapy in non-small cell lung cancer. J Thorac Oncol. 2007; 2:S101–S112. [PubMed: 17603304]
16. Stanic S, Paulus R, Timmerman RD, et al. No clinically significant changes in pulmonary function following stereotactic body radiation therapy for early-stage peripheral non-small cell lung cancer: An analysis of RTOG 0236. Int J Radiat Oncol Biol Phys. 2014; 88:1092–1099. [PubMed: 24661663]
17. Timmerman R, Paulus R, Galvin J, et al. Stereotactic body radiation therapy for inoperable early stage lung cancer. JAMA. 2010; 303:1070–1076. [PubMed: 20233825]
18. Matinfar M, Ford E, Iordachita I, et al. Image-guided small animal radiation research platform: Calibration of treatment beam alignment. Phys Med Biol. 2009; 54:891–905. [PubMed: 19141881]
19. Hong ZY, Eun SH, Park K, et al. Development of a small animal model to simulate clinical stereotactic body radiotherapy-induced central and peripheral lung injuries. J Radiat Res. 2014; 55:648–657. [PubMed: 24556815]
20. Otani T, Otsuka H, Kondo K, et al. Utility of respiratory-gated small-animal PET/CT in the chronologic evaluation of an orthotopic lung cancer transplantation mouse model. Radiol Phys Technol. 2015; 8:266–277. [PubMed: 25921487]
21. Bissonnette JP, Purdie TG, Higgins JA, et al. Cone-beam computed tomographic image guidance for lung cancer radiation therapy. Int J Radiat Oncol Biol Phys. 2009; 73:927–934. [PubMed: 19095368]
22. Rodriguez M, Zhou H, Keall P, et al. Commissioning of a novel microCT/RT system for small animal conformal radiotherapy. Phys Med Biol. 2009; 54:3727–3740. [PubMed: 19478377]

23. Sweet-Cordero A, Mukherjee S, Subramanian A, et al. An oncogenic KRAS2 expression signature identified by cross-species gene-expression analysis. Nat Genet. 2005; 37:48–55. [PubMed: 15608639]

24. Westcott PM, Halliwill KD, To MD, et al. The mutational landscapes of genetic and chemical models of Kras-driven lung cancer. Nature. 2015; 517:489–492. [PubMed: 25363767]

25. Tam IY, Chung LP, Suen WS, et al. Distinct epidermal growth factor receptor and KRAS mutation patterns in non-small cell lung cancer patients with different tobacco exposure and clinicopathologic features. Clin Cancer Res. 2006; 12:1647–1653. [PubMed: 16533793]

26. Rodenhuis S, Slebos RJ. Clinical significance of ras oncogene activation in human lung cancer. Cancer Res. 1992; 52:2665s–2669s. [PubMed: 1562997]

27. Elsum IA, Yates LL, Pearson HB, et al. Scrib heterozygosity predisposes to lung cancer and cooperates with KRas hyperactivation to accelerate lung cancer progression in vivo. Oncogene. 2014; 33:5523–5533. [PubMed: 24276238]

28. Burnette B, Weichselbaum RR. The immunology of ablative radiation. Semin Radiat Oncol. 2015; 25:40–45. [PubMed: 25481265]

29. Formenti SC, Demaria S. Systemic effects of local radiotherapy. Lancet Oncol. 2009; 10:718–726. [PubMed: 19573801]

30. Dewan MZ, Galloway AE, Kawashima N, et al. Fractionated but not single-dose radiotherapy induces an immune-mediated abscopal effect when combined with anti-CTLA-4 antibody. Clin Cancer Res. 2009; 15:5379–5388. [PubMed: 19706802]

Summary

This work demonstrates the feasibility of using human stereotactic body radiation therapy (SBRT) protocols to deliver image guided SBRT treatments in rodent models using a small animal irradiator. The use of genetically engineered mice with *Kras*-driven spontaneous lung tumors that closely mimic human non-small cell lung cancer is a unique preclinical model for SBRT. We have demonstrated that SBRT can be precisely delivered to murine lung peripheral tumors while sparing adjacent tissues and organs at risk. In addition, we validated biological effects from SBRT in irradiated tissues. This novel platform provides new research opportunities that investigate the combination of SBRT with other therapeutic agents.

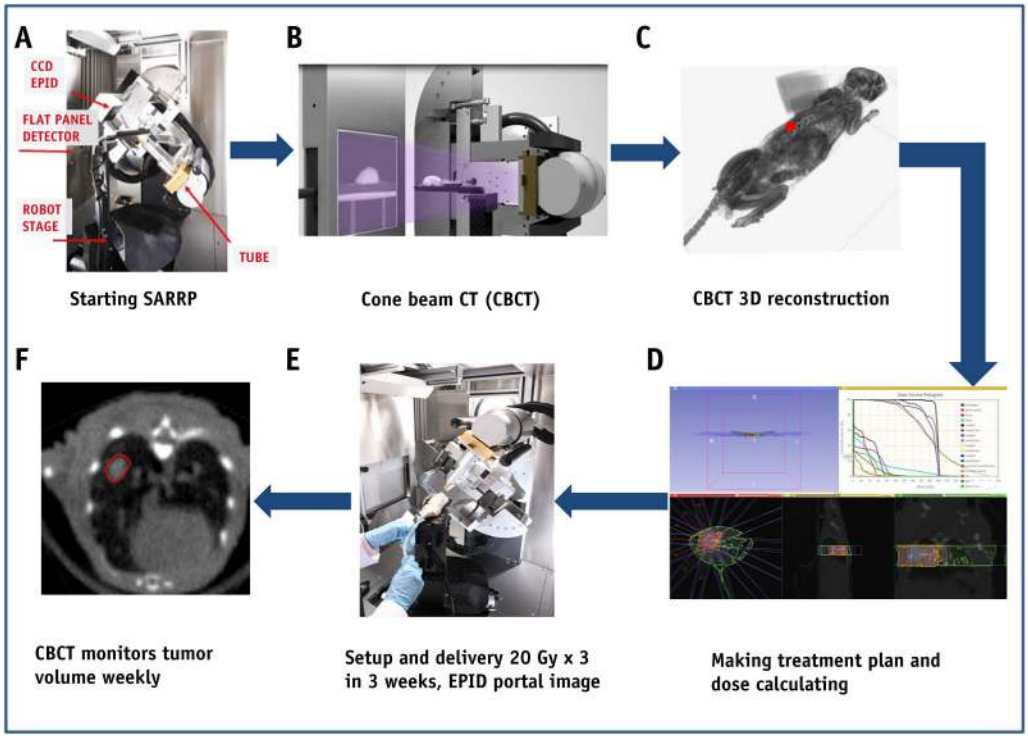

Fig. 1.

Stereotactic body radiation therapy (SBRT) in a transgenic lung cancer model on an Xstrahl small animal radiation research platform (SARRP). (A) The SARRP consists of a kilovoltage x-ray tube producing energy beams up to 225 kVp mounted on a rotating gantry. (B) Pretreatment onboard cone beam computed tomographic (CBCT) images were obtained at 60 kVp and 0.5 mA with an uncollimated primary beam. (C) The CBCT slices were rendered into a 3-dimensional (3D) reconstruction of the mouse. (D) MuriPlan, an image guided small animal dose planning system, was used to develop an SBRT treatment plan. (E) Three weekly fractions of 20 Gy were delivered to the right mouse lung. (F) CBCTs were taken each week during radiation therapy. *Abbreviation:* CCD = charge-coupled device, EPID = electronic portal imaging device.

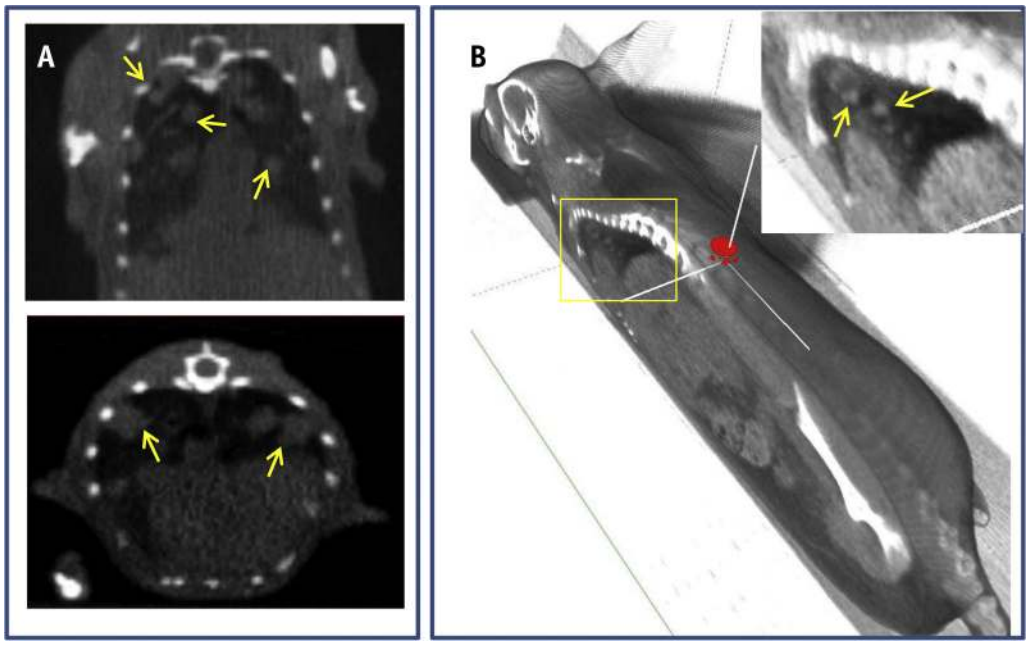

Fig. 2.

Cone beam computed tomographic (CBCT) imaging of a mouse model with *Kras*-driven lung cancer. (A) Coronal and transverse views through the thorax of a live mouse with multiple spontaneous *Kras*-driven tumors (yellow arrows). (B) Semitransparent 3-dimensional reconstruction of the same mouse, based on the virtual in vivo onboard CBCT slices. The spatial organization and localization of the tumor mass is highlighted by the yellow arrows. (A color version of this figure is available at www.redjournal.org.)

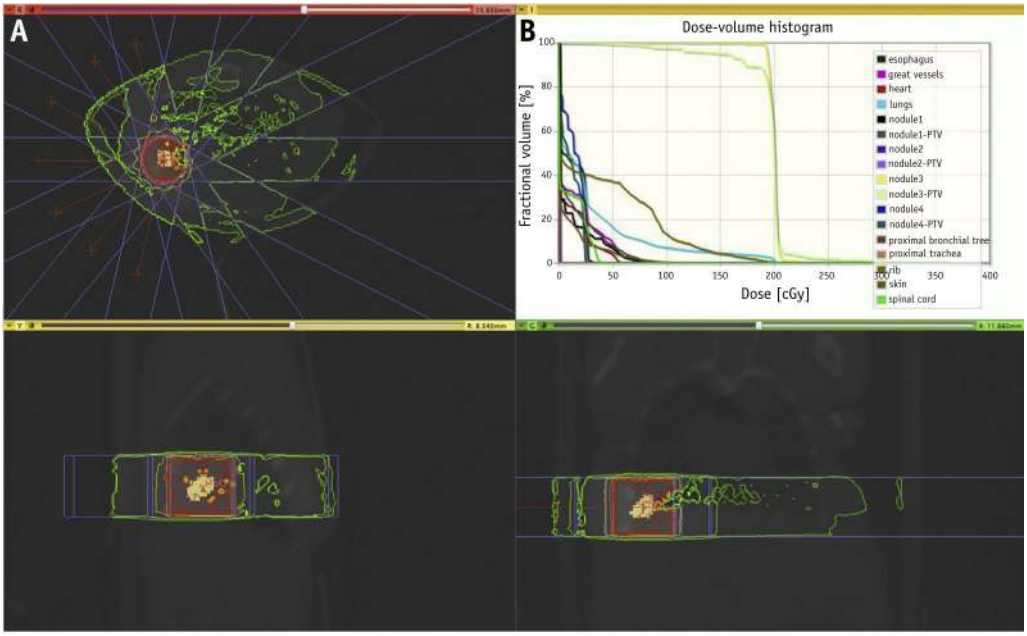

C

RTOG 0813 Conformality

	Mouse 1	Mouse 2	Mouse 3	Deviation: None	Deviation: Minor
PTV volume (cc)	**0.3043**	0.0868	0.4369	1.8	
Ratio of Rx isodose volume to the PTV volume	**1.95**	1.168	0.992	<1.2	<1.5
Ratio of 50% Rx isodose volume to the PTV volume, $R_{50\%}$	**5.15**	4.349	3.967	<5.9	<7.5
Maximum dose (in % of Rx) @ 2 mm from PTV in any direction, $D_{2\ mm}$(Gy)	**31.675**	53.3	55.9	<50.0	<57.0
Percent of lung receiving 20 Gy total or more, V_{20}(%)	**10.1**	3.72	18.5	<10	<15

Fig. 3.

Stereotactic body radiation therapy (SBRT) planning. (A) Cone beam computed tomographic scan of animal model, axial view (above), sagittal view (below, left), and coronal view (below, right), with simulation of radiation dose distribution around the treatment volume, beam angles (red lines), and static fields (flanking blue lines) using a 5 × 5–mm collimator. (B) Cumulative dose-volume histogram of tumor volume, normal lung tissue, and organs at risk. (C) Planning target volume (PTV), $R_{100\%}$, $R_{50\%}$, D_{2mm}, and V_{20} values for each animal model compared with the Radiation Therapy Oncology Group (RTOG) 0813 conformality protocol. (A color version of this figure is available at www.redjournal.org.)

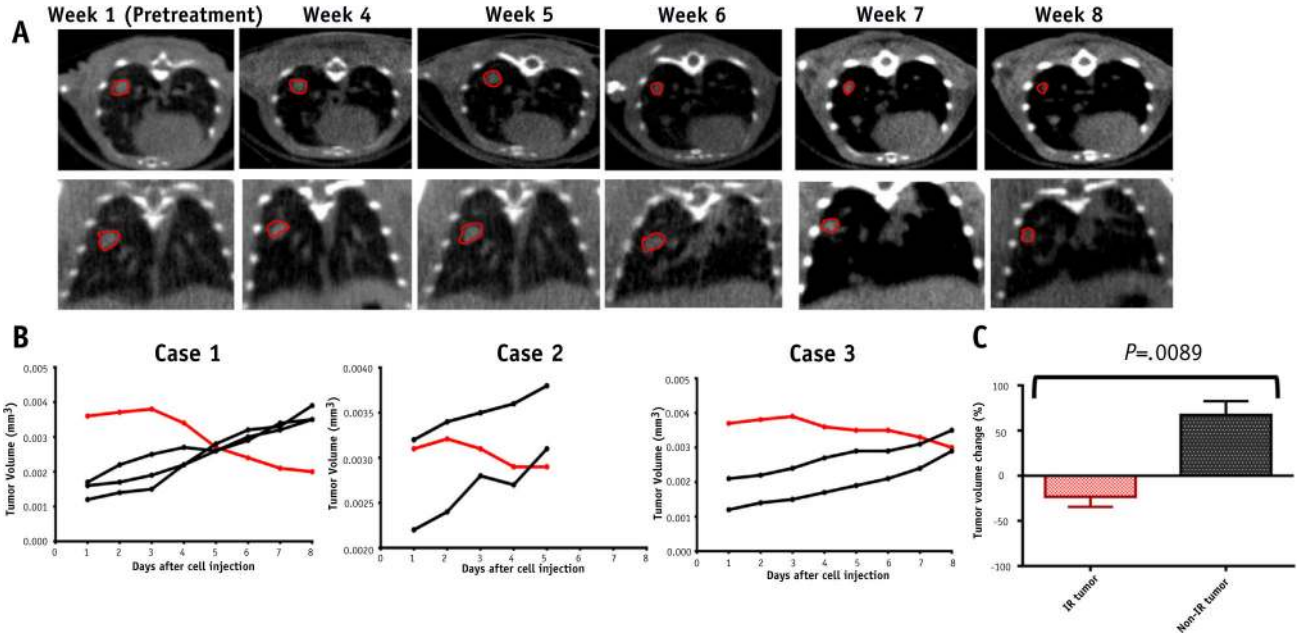

Fig. 4.

Radiographic response after sterotactic body radiation therapy (SBRT). (A) Pretreatment cone beam computed tomographic (CBCT) and weekly CBCT images after radiation therapy. Target irradiated tumor circled in red. (B) Evolution of tumor volumes in the 3 mouse models. Each line represents an individual tumor. Red lines represent the volume of the target irradiated tumor. Black lines represent the volume of the control tumors in the contralateral lung that received minimal radiation. (C) Tumor volume change 8 weeks after starting RT. Irradiated (IR) tumor n = 3; non-IR tumor n = 7. Data represent the average of 3 to 7 tumors ± standard error from 1 to 3 different mice. *P* values were calculated using a 2-tailed Student *t* test: $P<.05$. (A color version of this figure is available at www.redjournal.org.)

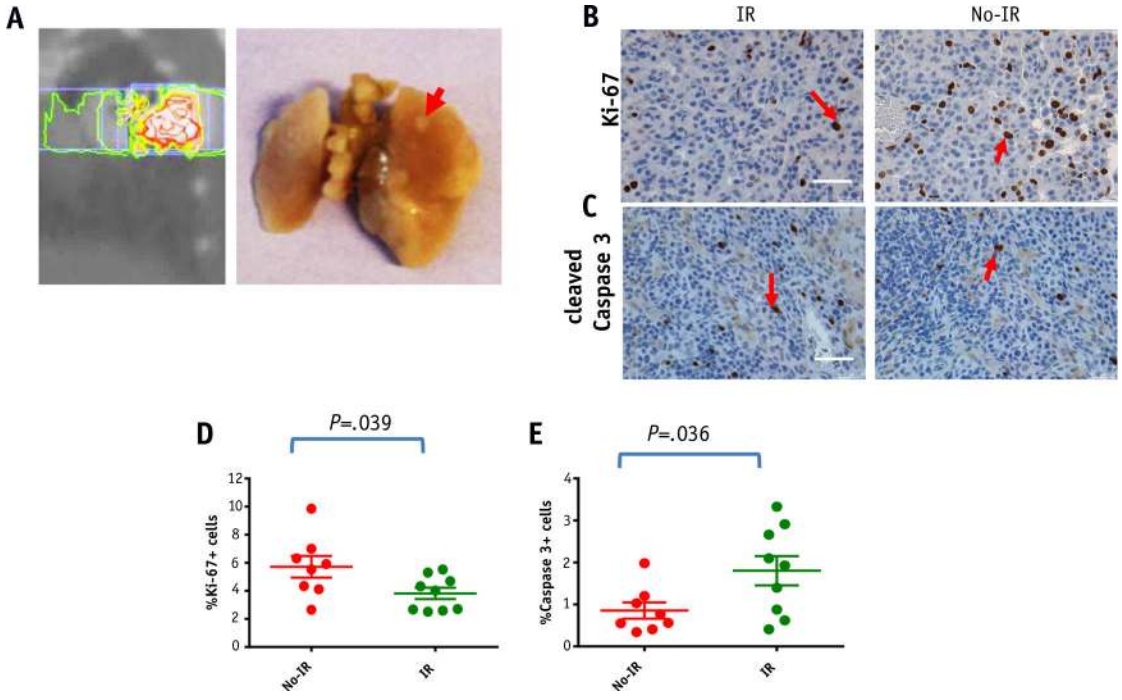

Fig. 5.

Pathologic response after stereotactic body radiation therapy. (A) Gross morphology. Mice were killed 5 weeks after radiation therapy. The peripheral right posterior lung nodule (plan at left) is indicated by the red arrow (right). (B, C) Immunohistochemical staining for Ki-67 (B) and caspase-3 (C) positive nuclei in target irradiated tumor tissue and control tumor tissue. Quantification of Ki-67 (D) and cleaved caspase-3 (E) positive cells in target versus control tumors. Data represent the average of 8 to 10 different fields ± standard error from 1 to 3 different mice. Scale bar represents 50 μm. *P* values were calculated using a 2-tailed Student *t* test $P<.05$. *Abbreviation:* IR = irradiation. (A color version of this figure is available at www.redjournal.org.)